Low Scattering Plane Wave Generator Design Using a Novel Non-coplanar Structure for Near-Field Over-the-air Testing

QIAO, ZHAOLONG ; WANG, ZHENGPENG ; Fan, Wei; ZHANG, XUE ; GAO, STEVEN ; MIAO, JUNGANG

Published in:
IEEE Access

DOI (link to publication from Publisher):
10.1109/ACCESS.2020.3039367

Publication date:
2020

Document Version
Publisher's PDF, also known as Version of record

IEEE Access
Multidisciplinary | Rapid Review | Open Access Journal

SPECIAL SECTION ON CHALLENGES AND ENDEAVORS OF RADIATED RADIO FREQUENCY TESTS FOR 5G RADIOS

Received November 4, 2020, accepted November 13, 2020, date of publication November 19, 2020,
date of current version December 7, 2020.

Digital Object Identifier 10.1109/ACCESS.2020.3039367

Low Scattering Plane Wave Generator Design Using a Novel Non-Coplanar Structure for Near-Field Over-the-Air Testing

ZHAOLONG QIAO[1], ZHENGPENG WANG[1], (Member, IEEE), WEI FAN[2], (Senior Member, IEEE), XUE ZHANG[1], STEVEN GAO[3], (Fellow, IEEE), AND JUNGANG MIAO[1]

[1]School of Electronic and Information Engineering, Beihang University, Beijing 100191, China
[2]Department of Electronic Systems, Aalborg University, 9100 Aalborg, Denmark
[3]School of Engineering and Digital Arts, University of Kent, Canterbury CT2 7NT, U.K.

Corresponding author: Zhengpeng Wang (wangzp@buaa.edu.cn)

This work was supported in part by the National Science and Technology Major Project under Grant 2018ZX03001028, and in part by NSFC under Grant 61671054.

ABSTRACT Plane Wave Generator (PWG) has recently attracted great attention from industry and academia for over-the-air (OTA) testing of base station (BS) antennas in the fifth-generation (5G) wireless communication systems. This paper aims to reduce the scattering from the PWG to the antenna under test (AUT), which might be problematic in the near-field OTA testing. First, we introduce a low monostatic radar cross section (RCS) PWG array element design. The PWG is also loaded with pyramidal microwave absorbing material (MAM) to suppress the multi-reflections between the AUT and the PWG. Furthermore, unlike coplanar PWG design generally reported in the literature, a novel non-coplanar design is proposed to realize the destructive interference of the scattered signals from the PWG, thereby significantly reducing the multiple reflections. PWG elements in the non-coplanar design are placed in the propagation direction according to planar and non-planar field distribution on the PWG radiated from the BS AUT. To validate our proposed design, a 4×4 PWG array with a 108 mm element spacing and a non-coplanar structure is developed and experimentally validated. The measured results show that the second incident wave of the proposed non-coplanar PWG array structure based on non-planar field distribution is 7.9 dB lower than that of the classical coplanar PWG design from 2.3 GHz to 3.8 GHz, and 1.9 dB lower than that of the proposed non-coplanar PWG array structure based on planar field distribution, which demonstrates the effectiveness and robustness of our proposed design.

INDEX TERMS 5G, OTA testing, PWG, low scattering design, probe antenna design, non-coplanar PWG structure.

I. INTRODUCTION

Massive multiple-input multiple-output (MIMO) is one of the key technologies employed at the base stations (BSs) in the sub-6 GHz 5G wireless communication systems [1], [2]. Accurate measurement of the massive MIMO BS antenna systems is essential in the performance and conformance testing. Over-the-air (OTA) testing is a competitive method to evaluate BS antennas due to its advantage of convenient operation and cost savings, compared to conventional cable conducted testing [3], [4]. The plane-wave generator (PWG), which aims to approximate a plane wave in the quiet zone with a near-field distance, has attracted great interest recently [5]–[10]. Compared with the traditional antenna measurement methods (e.g., near-field to far field transformation, direct far-field and compact antenna testing range (CATR)), the PWG has the advantages of compact size, fast measurement, low-cost, and support for both continuous wave (CW) and modulated signal measurement. The PWG has a good potential to support for massive MIMO BS antenna parameter measurement, array calibration, radio frequency (RF) transmit and receive performance measurements.

Extensive works have been reported on the PWG design in the literature, e.g. algorithms to determine the complex excitation coefficients for the PWG element [11]–[13], and

The associate editor coordinating the review of this manuscript and approving it for publication was Shah Nawaz Burokur.

guidance to design a good PWG [14]. Multiple reflections between the PWG and AUT will be detrimental to high-fidelity quiet zone performance, which is especially problematic due to the near-field measurement distance and metallic ground plane usually employed in the 5G BS AUT [15], [16]. However, this issue is largely overlooked in the PWG design in the literature. Due to the immutable BS AUT design, the most efficient way to suppress the multiple reflections between PWG and BS AUT is to reduce the scattering from the PWG.

Scattering reduction has been a long-standing research topic in the literature in the near-field measurement systems, where various techniques, e.g. data post-processing, downsizing the cross-section of probe antenna, and diverting the direction of the reflected wave, have been reported. A mathematical absorber reflection suppression (MARS) technique was used in [17] to suppress the undesirable scattered signals, which is a post-processing technique using a digital filter technology. It was shown in [18] that wideband backscattering reduction can be achieved by miniaturizing the probe antenna with a compact wideband inverted quad ridge ortho-mode junction (OMJ). In [15], shaped expanded polypropylene absorbers surrounded by a taper slot antenna (TSA) were proposed and the back-scattering was reduced by absorbers. A conical skirt in front of the square probe frame was introduced in [19] to divert the energy scattered from the probe mounting structure away from the direction of the device under test (DUT). The miniaturized low scattering antennas were also reported in [16], [20], [21]. Some low scattering ground planes such as electromagnetic bandgap (EBG) and frequency selective surface (FSS) were introduced to replace the metal reflect board of antenna in [22], [23]. To reduce the scattering from the PWG, we need to carefully address the structural mode and antenna mode in the radar cross section (RCS) of the PWG antenna element [24], [25]. Furthermore, the ground plane of the PWG is another major factor, which should also be properly accounted for due to its large array aperture. For this reason, a low-scattering compact PWG probe antenna is designed in this paper, which is loaded with microwave-absorbing materials (MAMs) at its side edges to block the scattering in the sharp edge. The pyramidal shaped absorber is also introduced in the PWG to cover the large ground plane.

A chessboard structure is a promising strategy to reduce RCS, where the basic idea is that destructive interference can be realized to achieve scattering reduction. We can utilize a surface that reflects the impinging wave in-phase and counter-phase at the same time. This can be achieved via utilizing different properties of cells (i.e. one cell introducing 180° phase change to reflected wave, yet another cell introducing no phase change) on the surface. Artificial magnetic conductor (AMC) and perfect electric conductor (PEC) based chessboard structures were proposed in [26], [27]. Polarization conversion meta-surface (PCM) offers another approach to building the elements of a chessboard structure array [28]. It was also shown in [29] that the FSS could also be implemented in the chessboard arrangement. Note that planar wave impinging is generally assumed for the reported RCS reduction in the chessboard structure array.

Inspired by the chessboard structure reported in the literature, a novel non-coplanar PWG design is proposed in the paper to achieve destructive interference. Unlike coplanar PWG generally reported in the literature, the non-coplanar design can effectively suppress the reflected waves, without jeopardizing the PWG performance. The PWG elements in the non-coplanar design can be placed in the propagation direction according to planar field distribution or non-planar field distribution in the near-field region of the BS. To our best knowledge, such a low-scattering PWG design has not been available in the literature.

In this paper, several scattering reduction strategies are employed in the PWG design, i.e. low scattering probe antenna design, PWG ground plane covered with absorbing material, and a novel non-coplanar PWG layout based on field distribution. The paper is organized as follows. Section II introduces the low scattering PWG element design. Section III presents the low scattering PWG design. Section IV describes the non-coplanar PWG design for near-field field distribution. Section V draws conclusions.

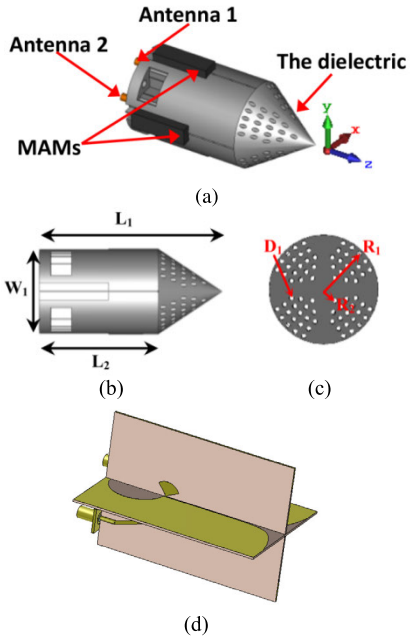

FIGURE 1. Geometry of the probe antenna: (a) the 3D view of the probe antenna; (b) the side view of the dielectric; (c) the front view of the dielectric; (d) the structure of Vivaldi antennas.

II. LOW SCATTERING PWG ELEMENT DESIGN

A. PWG ELEMENT DESIGN

Fig. 1 (a) presents the 3D view of the proposed PWG probe antenna, which consists of two crossed Vivaldi antennas, one dielectric, and radome and four MAM wings. The Vivaldi antenna and MAM wing structure were reported in our previous work [16], where a double-layer dielectric

TABLE 1. Detailed dimension of the proposed probe antenna.

Parameters	Values (mm)	Parameters	Values (mm)
L_1	113.82	D_1	2.4
L_2	73.82	R_1	24.75
W_1	53.4	R_2	7.78

structure was adopted. In this work, the only one-layer radome is employed in the design in order to improve the consistency of PWG antenna elements, without deteriorating the performance. The probe antenna dimension parameters are shown in Table 1. The Vivaldi antenna structure is shown in Figure 1(d). Vivaldi antenna 1 and 2 are defined in the yz-plane and xz-plane, respectively. Meanwhile, the two orthogonal antennas were inserted into the dielectric radome together, where a small distance difference in the z-axis exists to avoid overlapping in the microstrip lines. The substrate used to fabricate the Vivaldi antenna is Rogers (lossy, $\varepsilon_r = 3.38$) with a thickness of 0.813 mm. The sharp edge of the copper-clad plate of the Vivaldi antenna will lead to strong scattering, which is an important structure mode scattering. To alleviate this effect, the antenna edges are wrapped by four MAM wings of ECCOSORB LS-26 (as shown in Fig. 1(a)) with "U-shape". The dielectric radome has a nearly rotational symmetry structure, with a cylindrical body and a cone head as shown in Fig. 1(a) and (b). The conehead can effectively divert the incident wave to a non-boresight direction. 76 holes are penetrated in circles in the dielectric radome to reduce weight. The dielectric permittivity of polylactic acid (PLA), which has been used to fabricate the radome, is 2.6. Table 2 shows the loss factors of the MAM, Rogers substrate, and the radome used in the simulation from the CST. The antenna geometry is simulated and optimized in the full-wave electromagnetic simulation software CST.

TABLE 2. The loss factors of the Mam, the rogers substrate, and the radome used in the simulation.

Components	Frequency (GHz)	Loss Factor
MAM	2.6	19.497427
	3.5	16.069471
	4.9	12.823218
Rogers Substrate	2.6	0.008815
	3.5	0.008775
	4.9	0.009005
Radome	2.6	0.000193
	3.5	0.000192
	4.9	0.000197

The fabricated probe antenna is shown in Fig. 2. The dielectric radome was processed by 3D printing technology, and the two Vivaldi antennas were perfectly inserted into the cross-shaped slot of the dielectric radome. Each MAM wing was glued by two dissected MAM strips. SMA connectors

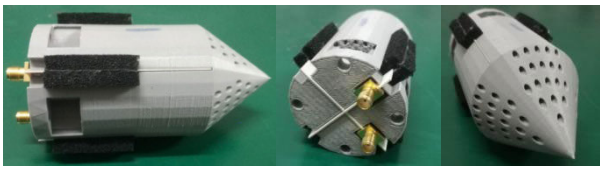

FIGURE 2. Photos of the fabricated probe antenna.

with a 0.8 mm inner radius were employed to the feed. The antenna can be easily installed in the ground plane by the four bottom through-holes, as shown in Fig. 2.

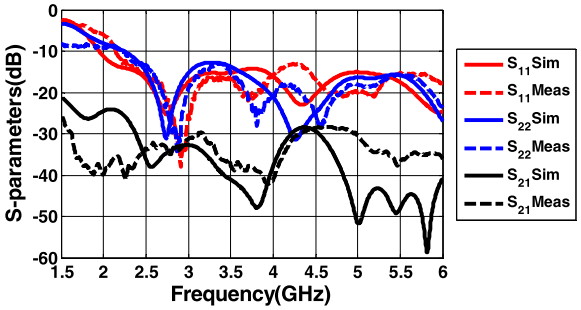

FIGURE 3. Simulated and measured S-parameters, S_{11}, S_{22} and S_{21} of the probe antenna.

B. THE SIMULATED AND MEASURED RESULTS OF THE PROBE ANTENNA

Simulated and measured S-parameters of the PWG probe antennas are shown in Fig. 3. The measured results agree well with the simulated results. The S_{11} and S_{22} of the compact probe antenna are improved by the loaded dielectric in the low frequency region, as expected. If the reflection coefficient less than -10 dB is targeted, the probe antenna could well support operating frequency from 2.2 GHz to 6 GHz for both antenna ports. The low reflection coefficients can be beneficial to the reduction of the RCS antenna mode. The high isolation between the two ports can also be achieved with the probe design, with $S_{21} < -20$ dB over the whole band, $S_{21} < -25$ dB at 2.2 GHz to 6 GHz band, and >30 dB isolation for most frequency regions.

Fig. 4 shows the measured and simulated radiation patterns along the *xz* and *yz* planes at 3.5 GHz. We can observe that measured radiation patterns match well the simulated results. Note that the back lobe is high due to the compact aperture size of the probe antenna.

Fig. 5 shows the simulated and measured monostatic RCS of the probe antenna in the gazing direction, and the measured RCS is less than -27.5 dBsm from 2.3 GHz to 3.8 GHz, which demonstrates a low-scattering probe antenna design. There is a big difference between measured and simulated RCS results. This is possibly due to the fact that the antenna material and antenna assembly are not accurately modeled in the simulation. The antenna is composed of components of different materials and the assembly of the antenna is done

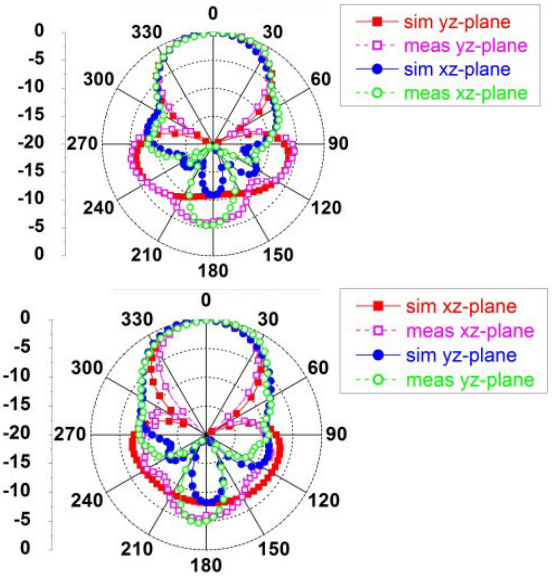

FIGURE 4. Simulated and measured antenna radiation patterns in the xz-plane and yz- plane at 3.5GHz. Top: antenna 1; Bottom: antenna 2.

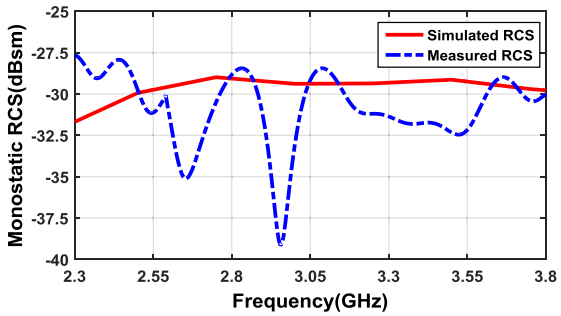

FIGURE 5. Monostatic RCS of the probe antenna in the gazing direction.

manually in the laboratory. The assembly accuracy of the antenna is limited, and gaps and position deviations will cause differences in RCS test results. In addition, the antenna is very small and the RCS level is rather low. The installation position of the antenna in the test will also slightly affect the measurement of scattered electromagnetic waves. The RCS of the probe antenna was measured in a CATR setup.

III. LOW SCATTERING PWG DESIGN

A. NON-COPLANAR PWG DESIGN FOR PLANAR IMPINGING WAVE

As explained, we aim to achieve destructive interference of reflected wave from the PWG with a novel non-coplanar PWG design. Coplanar PWG design (i.e. all PWG elements placed in the same *xy* plane) is generally adopted in the literature. In our work, non-coplanar PWG (i.e. PWG elements placed on two planes) is proposed in this section. The basic principle is explained below. For a certain frequency f, its wavelength is λ. Assume a planar wave impinging the PWG, a 180° phase change can be effectively generated for PWG elements if a change of $\lambda/4$ is introduced in the propagation path for the PWG element (back and forth (round trip) transmission distance of $\lambda/2$). Therefore, in our proposed non-coplanar PWG design, the PWG elements can be placed into two coplanar PWG planes, separated by a distance of $\lambda/4$. By doing so, the reflected waves from the whole PWG will be significantly suppressed due to the destructive interference of signals radiated from the PWG elements on the two planes at the frequency f (i.e. 180° phase difference introduced in the signal path). Note that the complex excitation coefficients are generally optimized for coplanar PWG design. Placing the PWG elements on two planes will therefore effectively modify the complex excitation coefficients allocated to the PWG elements. To address this, a compensation phase term of −90° (single-trip transmission distance of $\lambda/4$) should be introduced to complex coefficients obtained in the coplanar PWG design for PWG elements that are shifted $\lambda/4$ in the *z*-axis direction.

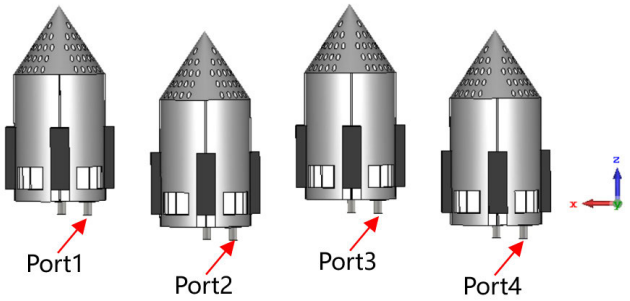

FIGURE 6. The schematic of the 1 × 4 non-coplanar array.

B. PWG ELEMENT SPACING DESIGN

In this work, uniform element spacing is adopted for the PWG design, though the proposed non-coplanar PWG strategy works for arbitrary PWG configuration. The element spacing of the non-coplanar structure is a key design parameter to achieve RCS reduction. Small element spacing would lead to large coupling between the elements, which would jeopardize the scattering reduction performance in the PWG due to strong coupling. A 1 × 4 non-coplanar array was simulated in the CST to determine the suitable PWG element spacing, as shown in Fig. 6. Four probe antennas were uniformly arranged in the x axis, with $\lambda/4$ separation for a neighboring element in the z-axis direction (for the designed frequency), as illustrated in Fig. 6. Fig. 7 presents the monostatic RCS reduction of the 1 × 4 non-coplanar array with different element spacings. Note that the results were normalized to the RCS of the coplanar PWG design for the four elements. The non-coplanar PWG design can effectively reduce the RCS, as expected. Furthermore, as the element spacing gets larger, better RCS reduction can be obtained at 2.6 GHz and 3.5 GHz, which is expected since we have smaller coupling due to larger element spacing. Nevertheless, with the frequency grows further, the RCS reduction tends to

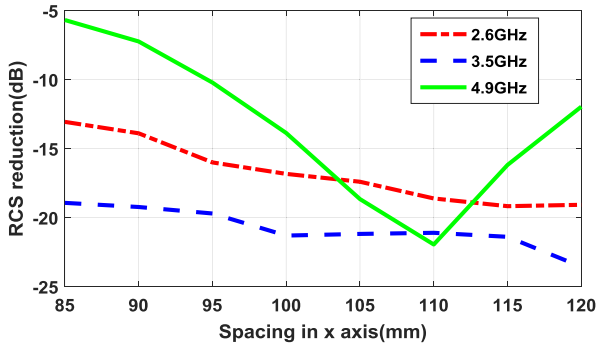

FIGURE 7. The monostatic RCS reduction of the 1 × 4 non-coplanar array in the different spacing.

be unstable at large element spacing. An element spacing of 108 mm is selected in the next section since it is a good choice both for PWG design in terms of plane wave field synthesis and also it offers good RCS reduction.

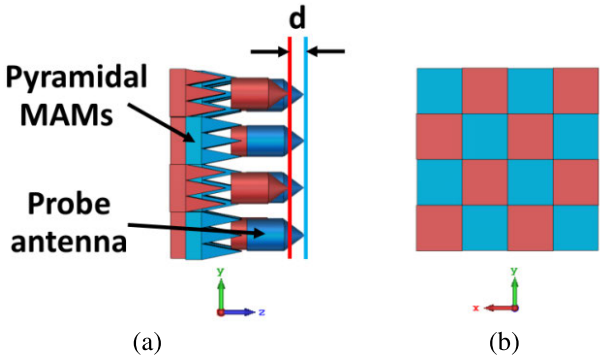

FIGURE 8. The schematic of the non-coplanar PWG: (a) the side view and (b) the back view.

C. NON-COPLANAR PWG IMPLEMENTATION

For simplicity, a 4 × 4 PWG is developed for validation purpose, though the principle can be applied for PWG of arbitrary size. The non-coplanar PWG consists of 16 low scattering antenna elements, as illustrated shown in Fig. 8. The distance between two PWG planes in the z axis is set to d. One PWG element is composed of one probe antenna and a 3 × 3 pyramidal MAM, with the probe antenna placed ahead of the pyramidal MAM. The blue element is placed ahead of the red element in the z axis, as explained.

The prototype of the non-coplanar PWG structure is shown in Fig. 9, and the material of the backboards is aluminum. The MAM, which was used in the PWG, is the carbon loaded urethane foam absorber, whose whole height is 100 mm. The absorber element has the pyramidal shape, where the height of the pyramid is 70 mm, and the width of the base is 38.5 mm. Each probe antenna was propped by four polyamide 66 dielectric poles, and the pointing angle of the PWG element can be finely tuned by the nuts in the head of dielectric poles. The spacing of probe antennas in the x axis and y axis is 108 mm, as explained. The 4 × 4 PWG configuration is realized by 20 positioning bolts and three backboards, as shown in Fig. 9. Each 3 × 3 pyramidal MAM bottom was glued to the backboard 3. All MAM absorbers were hung up by the 16 positioning bolts through the backboard 1 and backboard 2. The holes in the backboard 1 are threaded holes, and locations of PWG elements can be adjusted by rotating the positioning boles. The remaining four positioning boles in the backboard 1 can be used to adjust the direction angles of backboard 2, and then the whole perpendicularity of the array can be compensated by backboard 2 with 16 precise through holes.

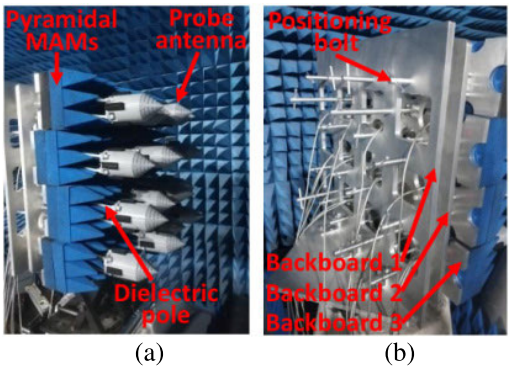

FIGURE 9. The prototype of the non-coplanar PWG: (a) the front view of the sub-array; (c) the back view of the sub-array.

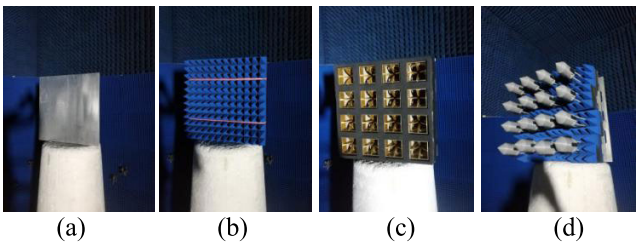

FIGURE 10. The different contrast models: (a) a flat metal plate; (b) a 12 × 12 pyramidal MAM array; (c) a 4 × 4 horn antenna array; (d) a 4 × 4 non-coplanar low-scattering probe antenna array.

To experimentally validate our proposed non-coplanar PWG design, four different models with the same aperture size 461.5 mm×461.5 mm are investigated to compare the reflectivity levels, as shown in Fig. 10. Note that all models are placed in the quiet zone of a CATR setup so that the planar signal impinging upon the models can be assumed. A flat aluminum metal plate, shown in Fig. 10 (a), is employed as the reference plate. All the other three models' reflectivity signals are normalized according to the reflection signal of the ideal metal plate. Fig. 10 (b) presents a 12 × 12 pyramidal MAM array, which is used as the initial background of the PWG array and backed by a metal plate. Fig. 10 (c) presents a 4 × 4 coplanar quad ridged horn antenna array, which is used as a conventional array to compare the reflectivity with the designed low scattering probe antenna array. The detailed dimensions of the horn antenna array were given in [30]. The

horn antenna array has an element spacing of 108 mm in the coplanar structure (i.e. with d = 0 mm). The gaps between the horn antennas were padded by planar foam absorbers. Fig. 10 (d) presents the designed 4 × 4 non-coplanar PWG, and the distance d in the z axis between adjacent elements was set to 0 mm, 15 mm, 20 mm, and 30 mm, respectively. All the array element ports in Fig. 10 (c) and Fig. 10 (d) were properly terminated to avoid potential port reflection.

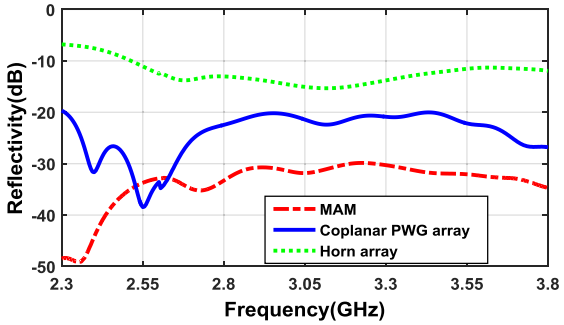

FIGURE 11. The reflectivity of different arrays.

All the models above were measured in a CATR setup. The reflectivity of different arrays is shown in Fig. 11. The reflectivity of MAM is less than −30 dB from 2.3 GHz to 3.8 GHz. Therefore, the pyramidal MAM array is suitable for low scattering background. An average difference between the three arrays is about 10 dB. In Fig. 11, the designed coplanar PWG array was arranged in a plane with $d = 0$ mm. The reflectivity of the PWG array is about 10 dB less than the horn antenna array, which demonstrates the low scattering property of the designed PWG element. The reflectivity of the MAM array mounts up about 10 dB due to the added probe antenna.

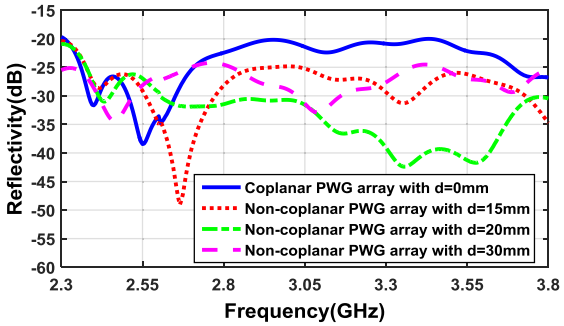

FIGURE 12. The reflectivity of non-coplanar PWG array with different adjustment distances.

Fig.12 represents the reflectivity of the designed non-planar PWG array with different distances in the z axis. When the d of the non-planar structure was set to 20 mm, the reflectivity was reduced by about 20 dB near the frequency of 3.5 GHz. This is due to the fact that 20 mm is approximately a quarter wavelength at 3.5 GHz (i.e. 21.4 mm). Compared with the planar array, 10 dB reflectivity suppression is achieved using the proposed non-planar structure with d = 20 mm from 2.8 GHz to 3.7 GHz. The measured results demonstrated that the proposed non-coplanar PWG design can significantly suppress the scattering from the PWG.

IV. NON-COPLANAR PWG DESIGN FOR NEAR-FIELD DISTRIBUTION

In Section III, a non-coplanar PWG is proposed based on the assumption that the PWG is illuminated by a planar impinging wave. It was demonstrated that the PWG scattering can be significantly reduced via placing PWG elements on two planes separated by $\lambda/4$ (for the designed frequency). However, the PWG is generally placed in the near-field region of the BS (e.g. the measurement distance can be as small as 2 times of the quiet zone size). Its compactness is one of the main advantages of the CATR solution. Due to the near-field distance, the field distribution on the PWG aperture radiated from the BS AUT is not an ideally uniform plane wave field. Therefore, the proposed non-coplanar PWG based on plane wave field distribution in Section III might deteriorate in the practical near-field setup. To address this issue, a non-coplanar PWG design strategy based on near field (typically non-planar) field distribution is proposed. Note that the plane wave field distribution can be viewed as a simplified case of the near-field field distribution for the non-coplanar PWG design.

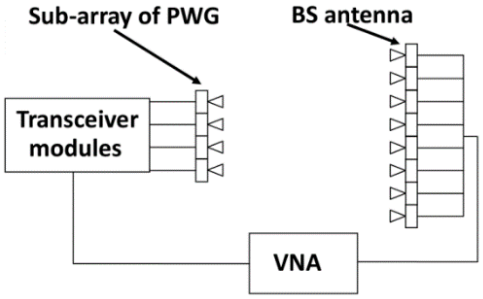

FIGURE 13. The schematic of the measurement system for non-coplanar PWG.

A. MEASUREMENT SYSTEM

The measurement setup is illustrated in Fig. 13. The PWG and BS AUT were installed face-to-face. A two-port vector network analyzer (VNA) is used to obtain the S_{21} response of the measurement system. A transceiver module, which can control the amplitude and phase of each PWG element, was cascaded between the PWG and VNA. Fig. 14 presents the location relations for the PWG and BS arrays in the measurement system. The BS antenna array (i.e., blue square array) is a 4 × 8 antenna array with the element spacing is 108 mm. The power splitter on the BS arrays side combines 32 antenna signals into one channel and connects to the VNA through longer cables. Note that the PWG array is offset from the coordinate origin in the measurement system, as shown in Fig. 14 and later in Fig. 15 to Fig. 17.

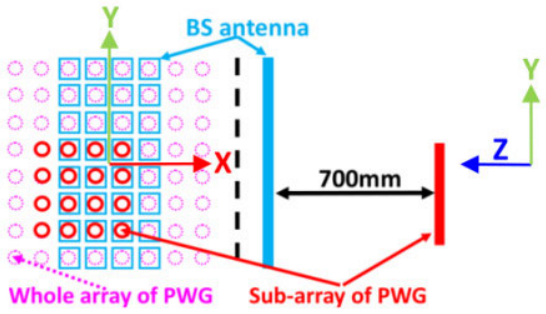

FIGURE 14. The location relations among the arrays.

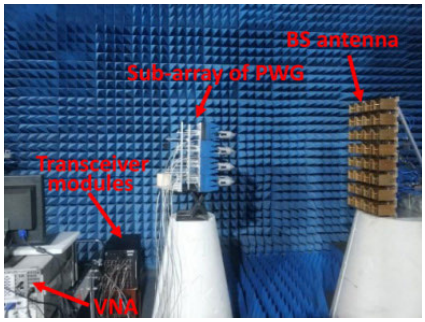

FIGURE 15. The experimental setup of the measurement system for non-coplanar PWG sub-array.

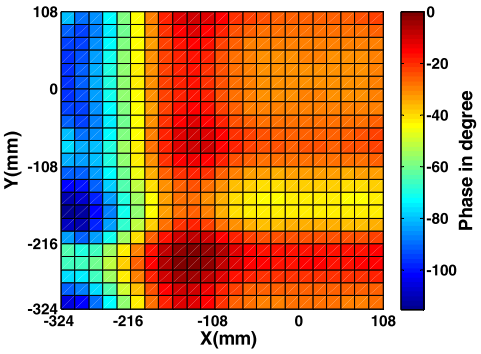

FIGURE 16. The phase distributions of incident field on the PWG array.

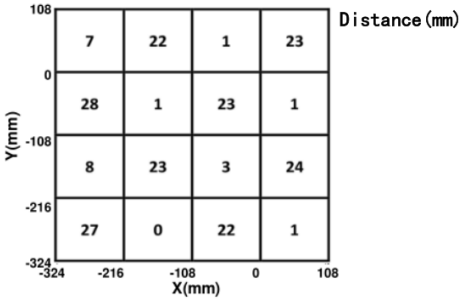

FIGURE 17. The distance differences of array element in the z axis.

To experimentally validate our proposed non-coplanar structure PWG, a small 4 × 4 PWG was chosen for the sake of simplicity. The PWG (i.e., red annulus array in Fig. 14) is a part of the whole array of PWG (i.e., pink annulus array). The distance of two arrays in the z axis is 700 mm, and it is a near-field distance for the BS antenna array at 3.5 GHz. Fig. 15 presents the experimental setup of the measurement system. The element of the BS antenna is the quad-ridged horn antenna as mentioned in Section III, and they were connected with another port of VNA by cascaded power dividers. The VNA was not calibrated during the whole process. The relative position of the reflected waves can still be accurately measured. The bandwidth of the transceiver module is from 2.3 GHz to 3.8 GHz, which agrees well with the supported frequency band of the antennas. The PWG design is detailed in Section III. The main contribution of this part is the design of non-coplanar PWG based on the near-field field distribution, as discussed below.

B. NON-COPLANAR PWG DESIGN FOR NON-PLANAR FIELD

The first step is to obtain the field radiated from the BS AUT over the PWG aperture. For a known BS AUT, its radiated field over the PWG aperture can be simulated by electromagnetic simulation software. For an unknown BS AUT, the field distribution can be measured with the help of a planar near-field scanner. In this work, the non-planar field distribution over the PWG aperture is simulated in the CST and FEKO software, which is shown in Fig. 16 at 3.5 GHz. The field distribution is not planar due to the near-field distance, as expected. The phase distribution is not uniform and a deviation up to 120° can be observed.

The next step is to subdivide the simulated field over the PWG aperture into 16 separate sections, according to the area of the PWG elements. The field in each section is then averaged. The phase distribution of the average field includes 16 separate sections (denoted as φ_n^{inc} for $n \in [1, 16]$). Note that for planar impinging wave, we have the same φ_n^{inc} for $n \in [1, 16]$.

As explained, the basic idea of non-coplanar PWG design is to achieve destructive interference by designing positions of PWG elements in the propagation direction (i.e. the z axis). The phase distribution of the objective field can be denoted as φ_n^{obj} for $n \in [1, 16]$. As explained, the field radiated by neighboring PWG elements should have the same amplitude, yet out-phased (i.e. phase difference of 180°). Therefore, we can set φ_n^{obj} for $n \in [1, 16]$ accordingly. Note that the amplitude distribution of the field is assumed uniform in the work.

Therefore, the phase adjustment for the n-th PWG element for $n \in [1, 16]$ can be written as

$$\varphi_n^{adj} = \varphi_n^{obj} - \varphi_n^{inc} \tag{1}$$

The phase adjustment can be either realized by tuning the phase shifter connected to each PWG element or adjusting the position of the PWG element in the z axis in principle. However, for the PWG application, the phase and amplitude excitation coefficients are optimized and should be fixed to approximate a plane wave in the quiet zone. If altered, the quiet zone performance will deteriorate. Therefore, we can

only realize the element phase adjustment with the proposed non-coplanar design of the PWG. The corresponding position adjustment of PWG element d_n^{adj} for $n \in [1, 16]$ in the z axis can be calculated as

$$d_n^{adj} = \frac{\varphi_n^{adj} \times \lambda}{2\pi \times 2} \tag{2}$$

where λ is the wavelength at 3.5 GHz. The factor of two in (2) is due to the back-and-forth transmission of the signal path, as explained. Fig. 17 presented the corresponding distance differences of the PWG element in the z axis in the proposed non-coplanar design. As explained, the phase excitation coefficients are effectively altered by moving the PWG elements in the z-axis. To maintain the same quiet zone performance as in the coplanar PWG design, we need to compensate for the phase shift introduced by the position adjustment of PWG elements. The compensated phase for the n-th for $n \in [1, 16]$ PWG element can be calculated as:

$$\phi_n^{com} = \frac{-\varphi_n^{adj}}{2} \tag{3}$$

By arranging the position of the PWG elements in the z-axis according to the near field distribution (i.e. (1) and (2)) and adjusting the phase excitation coefficients for the PWG elements (3), we can effectively suppress the scattering from the PWG, without affecting the PWG quiet zone performance.

Note that the PWG elements are placed on two planes in the non-coplanar PWG design with planar field distribution. The separation between two planes is set to $\lambda/4$ (for the designed frequency). However, in the non-coplanar PWG design with non-planar field distribution, all PWG element locations are determined based on the field distribution. The field distribution should be either simulated or measured.

C. VALIDATION MEASUREMENT

To evaluate the effectiveness of our proposed non-coplanar PWG design, a validation measurement is performed, where three PWG designs were evaluated, i.e., the traditional coplanar PWG, non-coplanar PWG for the planar distributed field, and non-coplanar PWG for the non-planar distributed field. As explained, the main difference lies in the positions of PWG elements in the z-axis in the PWG.

The level of scattering from the PWG can be recorded in the second incident wave to the PWG in the S_{21} response. The first incident wave to the PWG will be reflected back to the BS AUT, and then reflected back from the BS AUT to the PWG. Therefore, the second incident wave will lag behind the direct incident wave in the time domain, with a difference of 4.7 ns (corresponding to a propagation distance of 1400 mm). Fig. 18 presents the normalized S_{21} response of the measurement system in the time domain for different PWG designs, where a second incidence wave can be clearly observed. The proposed non-coplanar PWG design under planar field distribution is still valid in the near-field, where the peak value of the second incident wave is 6 dB lower than

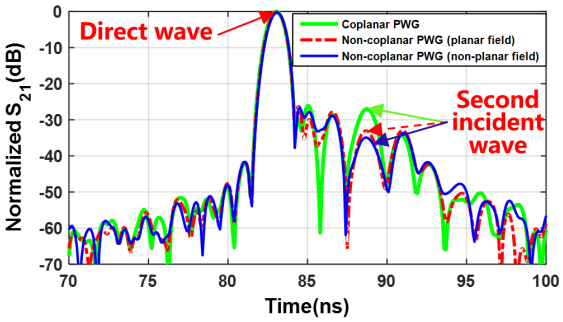

FIGURE 18. The normalized S_{21} response of measurement system in the time domain.

that with the traditional coplanar design. The non-coplanar PWG design under non-planar field distribution is 1.9 dB lower than the non-coplanar PWG design under planar field distribution, which demonstrated its effectiveness in further suppressing the second incident wave. Besides, the PWG's primary incident wave time is 83ns, the second incident wave time is 88.7ns. The two incident wave time difference is 5.7 ns, which corresponds to 1.71 m, and the round trip distance between the PWG and the BS is 1.4 m, which means the difference between the two is 0.31 m. Therefore, the single-trip distance is 0.155 m, which might be due to the fact that the antennas on both sides are not ideal point sources and the equivalent phase center position is inside the aperture of each probe.

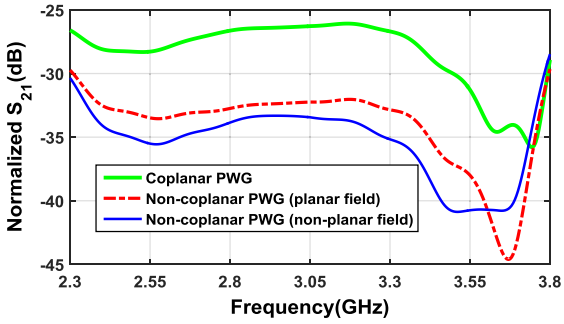

FIGURE 19. The normalized S_{21} response of measurement system in the frequency domain.

The non-coplanar PWG is designed for 3.5 GHz. It would be of interest to understand how large bandwidth the proposed design supports. For this purpose, we looked into the normalized S_{21} response of the measurement system in the frequency domain. Fig. 19 presents the normalized S_{21} response of the measurement system in the frequency domain. Time gating technique can be employed to extract the direct incident wave and second incident wave [31]. We use a time gating window of 5 ns and 2 ns to extract the direct and second incident wave, respectively. The level of the second incident wave in the non-coplanar PWG design under the non-planar wave at 3.5 GHz is -40.9 dB compared with the direct incident wave, which is about 3.7 dB better

than the non-coplanar PWG design under a planar wave at 3.5 GHz. We can also observe that although the non-coplanar PWG design under non-planar field is based on one single frequency, the scattering reduction around 2 dB and 7 dB also could be achieved from 2.3 GHz to 3.5 GHz, compared to the non-coplanar PWG design under planar field and coplanar PWG design, respectively.

A 14×9 non-planar array similar to the low scattering array is simulated to study the deterioration of quiet zone performance due to the introduction of non-coplanar PWG design, and the simulation results show that the proposed low scattering array can maintain the excellent plane wave performance of the planar PWG array.

V. CONCLUSION

PWG is an attractive over-the-air testing solution for massive MIMO BS antenna. However, its compact setup size would introduce multiple reflections between the PWG and the BS in the practical setup. To minimize this effect, several strategies were proposed and validated to reduce the scattering from the PWG. A compact and low-scattering probe antenna is designed for the PWG element, with RCS in the gazing direction less than -27.5 dBsm from 2.3 GHz to 3.8 GHz. An element spacing of 108 mm is selected for the uniform PWG design due to its low-scattering performance. The PWG ground plane is covered with absorbing material to reduce scattering as well due to the large PWG aperture. Furthermore, unlike coplanar PWG design generally proposed in the literature, we proposed a novel non-coplanar PWG design based on the destructive interference principle, which can significantly suppress the scattering of the PWG. Two non-coplanar PWG designs were proposed, one based on the planar field distribution and the other based on the non-planar field distribution.

Measurement results have demonstrated that the proposed non-coplanar PWG design under planar field distribution presents 6 dB suppression of scattering compared with the traditional coplanar design. The non-coplanar PWG design under non-planar field distribution can suppress the scattering further by 1.9 dB compared to the non-coplanar PWG design under planar field distribution, which demonstrated its effectiveness in further suppressing the second incident wave.

REFERENCES

[1] A. O. Martinez, J. O. Nielsen, E. De Carvalho, and P. Popovski, "An experimental study of massive MIMO properties in 5G scenarios," *IEEE Trans. Antennas Propag.*, vol. 66, no. 12, pp. 7206–7215, Dec. 2018.

[2] B. Yang, Z. Yu, Y. Dong, J. Zhou, and W. Hong, "Compact tapered slot antenna array for 5G millimeter-wave massive MIMO systems," *IEEE Trans. Antennas Propag.*, vol. 66, no. 12, pp. 6721–6727, Dec. 2017.

[3] H. Kong, Z. Wen, Y. Jing, and M. Yau, "Midfield over-the-air test: A new OTA RF performance test method for 5G massive MIMO devices," *IEEE Trans. Microw. Theory Techn.*, vol. 67, no. 7, pp. 2873–2883, Jul. 2019.

[4] P. Kyosti, W. Fan, G. F. Pedersen, and M. Latva-Aho, "On dimensions of OTA setups for massive MIMO base stations radiated testing," *IEEE Access*, vol. 4, pp. 5971–5981, 2016.

[5] F. Scattone, D. Sekuljica, A. Giacomini, F. Saccardi, J. Acree, J. Estrada, and L. J. Foged, "Dual polarized plane wave generator design for direct far-field testing," in *Proc. IEEE Int. Symp. Antennas Propag. USNC-URSI Radio Sci. Meeting*, Jul. 2019, pp. 1–4.

[6] F. Scattone, D. Sekuljica, A. Giacomini, F. Saccardi, A. Scannavini, L. J. Foged, E. Kaverine, N. Gross, and P. O. Iversen, "Comparative testing of devices in a spherical near field system and plane wave generator," in *Proc. Antenna Meas. Techn. Assoc. Symp. (AMTA)*, Oct. 2019, pp. 1–2.

[7] R. Xie, X. Wang, R. Wang, T. Wang, D. Chen, T. Song, and L. K. S. Zhu, "Synthesis of plane wave applied to 5G communication antenna measurement," in *Proc. Prog. Electromagn. Res. Symp. Spring (PIERS)*, St. Petersburg, Russia, May 2017, pp. 195–198.

[8] X. Sun, Z. Wang, and J. Miao, "Near field quasi plane wave generation and performance evaluation," in *Proc. Asia–Pacific Microw. Conf. (APMC)*, Kyoto, Japan, Nov. 2018, pp. 917–919.

[9] X. Zhang, Z. Zhang, and Y. Ma, "5G antenna system OTA testing with plane wave generator in range-constrained anechoic chamber," in *Proc. 6th Asia–Pacific Conf. Antennas Propag. (APCAP)*, Xi'an, China, Oct. 2017, pp. 1–3.

[10] M. Poordaraee and A. A. Glazunov, "Plane wave synthesis with irregular chamber planar antenna arrays for compact OTA measurements," in *Proc. 13th Eur. Conf. Antennas Propag. (EuCAP)*, Apr. 2019, pp. 1–5.

[11] M. D'Urso, G. Prisco, and M. Cicolani, "Synthesis of plane-wave generators via nonredundant sparse arrays," *IEEE Antennas Wireless Propag. Lett.*, vol. 8, pp. 449–452, 2009.

[12] O. M. Bucci, M. D. Migliore, G. Panariello, and D. Pinchera, "An effective algorithm for the synthesis of a plane wave generator for linear array testing," in *Proc. IEEE Int. Symp. Antennas Propag.*, Jul. 2012, pp. 1–2.

[13] O. M. Bucci, M. D. Migliore, G. Panariello, and D. Pinchera, "On the synthesis of plane wave generators: Performance limits, design paradigms and effective algorithms," in *Proc. 6th Eur. Conf. Antennas Propag. (EUCAP)*, Mar. 2012, pp. 3500–3503.

[14] O. M. Bucci, M. D. Migliore, G. Panariello, and D. Pinchera, "Plane-wave generators: Design guidelines, achievable performances and effective synthesis," *IEEE Trans. Antennas Propag.*, vol. 61, no. 4, pp. 2005–2018, Apr. 2013.

[15] J. Wu, Y. Qi, W. Yu, L. Liu, and F. Li, "An absorber-integrated taper slot antenna," *IEEE Trans. Electromagn. Compat.*, vol. 59, no. 6, pp. 1741–1747, Dec. 2017.

[16] Z. Qiao, Z. Wang, T.-H. Loh, S. Gao, and J. Miao, "A compact minimally invasive antenna for OTA testing," *IEEE Antennas Wireless Propag. Lett.*, vol. 18, no. 7, pp. 1381–1385, Jul. 2019.

[17] A. C. Newell and G. Hindman, "Scattering reduction in spherical near-field measurements," in *Proc. IEEE Antennas Propag. Soc. Int. Symp.*, San Diego, CA, USA, Jul. 2008, pp. 1–4.

[18] A. Giacomini, V. Schirosi, R. Morbidini, L. J. Foged, J. Estrada, J. Acree, and L. M. Tancioni, "Dual-polarized probe with full octave bandwidth and minimum scattering for planar near field measurements," in *Proc. Antenna Meas. Techn. Assoc. Symp. (AMTA)*, Atlanta, GA, USA, Oct. 2017, pp. 1–5.

[19] A. Frandsen, S. Pivnenko, and O. Breinbjerg, "Control of scattering from probes for near-field antenna measurements by use of skirt," *Electron. Lett.*, vol. 40, no. 5, pp. 284–285, Mar. 2004.

[20] L.-N. Chen, Y.-C. Jiao, H.-H. Xie, and F.-S. Zhang, "Minkowski fractal patch antenna for size and radar cross-section reduction," in *Proc. IEEE CIE Int. Conf. Radar*, Chengdu, China, Oct. 2011, pp. 1406–1409.

[21] P. Zhang and J. Li, "Compact UWB and low-RCS Vivaldi antenna using ultrathin microwave-absorbing materials," *IEEE Antennas Wireless Propag. Lett.*, vol. 16, pp. 1965–1968, 2017.

[22] W. Xing, T. Hong, W. Jiang, S. Gong, and Y. Li, "UWB Vivaldi array using frequency selective surface for low RCS applications," in *Proc. Int. Symp. Antennas Propag. (ISAP)*, Okinawa, Japan, Oct. 2016, pp. 474–475.

[23] Q. Chen, H. Zhang, X. Zhang, M. Jin, and W. Wang, "Wideband RCS reduction of vivaldi antenna using electromagnetic band gap absorbing structure," in *Proc. Int. Symp. Antennas Propag. (ISAP)*, Phuket, Thailand, Oct. 2017, pp. 1–2.

[24] F. Wang, W. Jiang, S. Gong, Y. Zhang, T. Hong, and H. Xue, "Radar cross section reduction of wideband antenna with a novel wideband radar absorbing materials," *IET Microw., Antennas Propag.*, vol. 8, no. 7, pp. 491–497, May 2014.

[25] E. F. Knott, J. F. Shaeffer, and M. T. Tuley, *Radar Cross Sections*, 2nd ed. Raleigh, NC, USA: SciTech, 2004.

[26] M. Paquay, J.-C. Iriarte, I. Ederra, R. Gonzalo, and P. de Maagt, "Thin AMC structure for radar cross-section reduction," *IEEE Trans. Antennas Propag.*, vol. 55, no. 12, pp. 3630–3638, Dec. 2007.

[27] J. Xue, W. Jiang, and S. Gong, "Chessboard AMC surface based on quasi-fractal structure for wideband RCS reduction," *IEEE Antennas Wireless Propag. Lett.*, vol. 17, no. 2, pp. 201–204, Feb. 2018.

[28] K. Li, Y. Liu, Y. Jia, and Y. J. Guo, "A circularly polarized high-gain antenna with low RCS over a wideband using chessboard polarization conversion metasurfaces," *IEEE Trans. Antennas Propag.*, vol. 65, no. 8, pp. 4288–4292, Aug. 2017.
[29] Y. Zheng, J. Gao, Y. Zhou, X. Cao, H. Yang, S. Li, and T. Li, "Wideband gain enhancement and RCS reduction of Fabry–Perot resonator antenna with chessboard arranged metamaterial superstrate," *IEEE Trans. Antennas Propag.*, vol. 66, no. 2, pp. 590–599, Feb. 2018.
[30] F. Zhang, W. Fan, Z. Wang, Y. Zhang, and G. F. Pedersen, "Improved over-the-air phased array calibration based on measured complex array signals," *IEEE Antennas Wireless Propag. Lett.*, vol. 18, no. 6, pp. 1174–1178, Jun. 2019.
[31] J. Knapp and T. F. Eibert, "Near-field antenna pattern measurements in highly reflective environments," *IEEE Trans. Antennas Propag.*, vol. 67, no. 9, pp. 6159–6169, Sep. 2019.

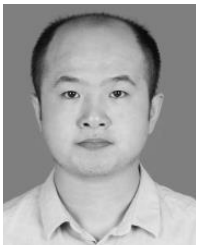

ZHAOLONG QIAO was born in Xingtai, China, in 1989. He received the B.E. degree from the Industrial and Commercial College, Hebei University, Baoding, China, in 2011, and the M.E. degree from the Hebei University of Science and Technology, Shijiazhuang, China, in 2014. He is currently pursuing the Ph.D. degree in electromagnetic filed and microwave technology with Beihang University, Beijing, China. Since 2014, he has been with the Electromagnetic Laboratory, Beihang University. His research interests include horn antennas, radar cross section testing, and over-the-air testing.

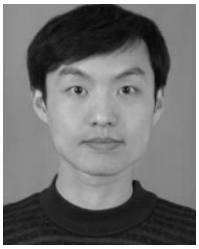

ZHENGPENG WANG (Member, IEEE) was born in Shandong, China, in 1981. He received the B.Sc. degree in electronic science and technology from Shandong University, Jinan, China, in 2004, and the M.Sc. and Ph.D. degrees in electromagnetic field and microwave technology from Beihang University, Beijing, China, in 2007 and 2012, respectively. He was a Visiting Researcher with the Antenna and Applied Electromagnetic Laboratory, University of Birmingham, Birmingham, U.K., from 2009 to 2010. From 2013 to 2015, he was a Research Fellow with the University of Kent, Canterbury, U.K., and the University of Science and Technology Beijing, Beijing. He is currently an Associate Professor with Beihang University. His current research interests include reconfigurable filters, reconfigurable antennas, filtering antennas, near-field antennas, and over-the-air testing.

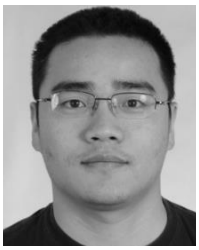

WEI FAN (Senior Member, IEEE) received the B.E. degree from the Harbin Institute of Technology, Harbin, China, in 2009, the master's double degrees (Hons.) from the Politecnico di Torino, Turin, Italy, and the Grenoble Institute of Technology, Grenoble, France, in 2011, and the Ph.D. degree from Aalborg University, Aalborg, Denmark, in 2014. In 2011, he joined Intel Mobile Communications, Aalborg, as a Research Intern. He conducted a three-month internship with Keysight Technologies, Oulu, in 2014. He is currently an Associate Professor with Aalborg University. His current research interests include over-the-air (OTA) testing of multiple antenna systems and radio channel sounding, parameter estimation, modeling, and emulation.

XUE ZHANG was born in Shandong, China, in 1997. She received the B.E. degree from the School of Information Engineering, China University of Geoscience, Beijing, China, in 2019. She is currently pursuing the M.E. degree in electromagnetic filed and microwave technology with Beihang University, Beijing. Since 2019, she has been with the Electromagnetic Laboratory, Beihang University. Her research interest includes compact antenna test range feed antenna.

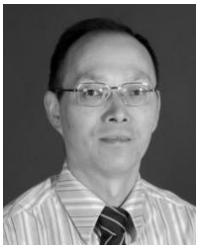

STEVEN GAO (Fellow, IEEE) received the Ph.D. degree in microwave engineering from Shanghai University, Shanghai, China, in 1999. He is currently a Full Professor and the Chair of RF and Microwave Engineering, and the Director of the Graduate Studies, School of Engineering and Digital Arts, University of Kent, Canterbury, U.K. He has coauthored or coedited three books, *Space Antenna Handbook* (Wiley, 2012), *Circularly Polarized Antennas* (the IEEE-Wiley, 2014), *Low-Cost Smart Antennas* (Wiley, 2019), and over 300 articles. He holds ten patents. He was an Invited Speaker with many conferences. His current research interests include smart antennas, phased arrays, MIMO, reconfigurable antennas, wideband/multi-band antennas, satellite antennas, RF/microwave/mm-wave/THz circuits, mobile communications, satellite communications, UWB radars, synthetic aperture radars, the Internet of Things (IoT), and sensors for healthcare. He is a Fellow of the Royal Aeronautical Society, U.K., and IET, U.K. He served as a Distinguished Lecturer for the IEEE AP Society. He served as the General Chair for LAPC in 2013. He serves as an Associate Editor for the IEEE TRANSACTIONS ON ANTENNAS AND PROPAGATION and several other international journals, such as *Radio Science*, IEEE ACCESS, *Electronics Letters*, *IET Circuits, Devices and Systems*, and so on. He serves as the Editor-in-Chief for John Wiley & Sons Book Series on *Microwave and Wireless Technologies*.

JUNGANG MIAO received the B.S.E.E. degree from the National University of Defense Technology, Changsha, China, in 1982, the M.S.E.E. degree from Beihang University, Beijing, China, in 1987, and the Dr.rer.nat. degree in physics from the University of Bremen, Bremen, Germany, in 1998. From 1982 to 1984, he was with the Institute of Remote Sensing Instrumentation, Chinese Aerospace, Beijing, where he developed spaceborne microwave remote sensing instruments. From 1984 to 1993, he was with the Electromagnetic Laboratory, Beihang University, where he has been a Chair Professor since 2003. In 1993, he joined the Institute of Environmental Physics and Remote Sensing, University of Bremen, as a Staff Member, where he was involved in research on spaceborne microwave radiometry. His research interests include electromagnetic theory, microwave engineering, and microwave remote sensing of atmosphere, including sensor development, calibration, and data analyses.